Finescale Surface Observations of the Dryline: A Mobile Mesonet Perspective

ALBERT E. PIETRYCHA

National Weather Service, Amarillo, Texas

ERIK N. RASMUSSEN

Cooperative Institute for Mesoscale Meteorological Studies, University of Oklahoma, Norman, Oklahoma

(Manuscript received 20 October 2003, in final form 2 June 2004)

ABSTRACT

Mobile mesonet line normal, time-to-space converted data analysis on three meridional drylines that occurred in west Texas on 10 June 1999 and 5 May 2000 are presented herein; two occurred in a quiescent environment on 5 May 2000. Based on the data, the mixing zone across the dryline was composed of a series of large horizontal moisture differentials that were highly variable in width, ranging from 5 km down to several hundred meters. The largest dewpoint differential sampled was 10.0°C over 185 m.

Concurrent with a deceleration of dryline movement to nearly stationary, and while moisture differentials strengthened, surface-based mesoscale vertical circulations with horizontal diameters of 2 km down to less than 300 m were resolved in the data, and visual observations were made of numerous, strongly rotating dust devils. The estimated diameters of the largest dust devils were ~80–100 m and ~1 km deep, and these persisted for tens of minutes. All vortices were found to move along or adjacent to the zones of moisture differential. Additionally, when the circulations were observed, spatially isolated cumulus clouds located along the dryline exhibited rapid vertical development. It is plausible that the vortices protect an ascending air parcel by inhibiting mixing, thus allowing the parcel to reach its local lifting condensation level and level of free convection with relatively greater buoyancy than parcels not contained in vortices.

1. Introduction

The Great Plains dryline frequently is a focal region for the initiation of deep, moist convection (Rhea 1966; Bluestein and Parker 1993). The *Glossary of Meteorology* defines the dryline as, ''A low-level mesoscale boundary or transition zone, hundreds of kilometers in length and up to tens of kilometers in width, separating dry air from moist air'' (Glickman 2000, p. 241). Typically, the moist air mass originates in the Gulf of Mexico and the dry air mass originates in the arid regions of the intermountain Southwest and subsides in the lee of the Rocky Mountains (Schaefer 1974b; Parsons et al. 1991). The dryline commonly develops over the southern and central Great Plains and is present on approximately 40% of spring and early summer days (Rhea 1966; Schaefer 1974b; Peterson 1983).

The dryline has been the focus of extensive study in past decades. A plethora of observational (e.g., NSSP Staff 1963; Hane et al. 1993, 1997; Crawford and Bluestein 1997; Atkins et al. 1998) and numerical (Schaefer 1974a; Sun and Wu 1992; Ziegler et al. 1995, 1997; Grasso 2000) studies have revealed a variety of thermodynamic and kinematic properties, and features embedded within the dryline such as mesoscale waves (McCarthy and Koch 1982). The research has provided insight into the behavior and structure of the dryline boundary.

Hane et al. (2001) separated dryline environments into two broad categories: synoptically active and quiescent. In the synoptically active environment, Great Plains drylines typically extend southward from a surface low pressure center. The motion of the dryline is driven by turbulent vertical mixing within the boundary layer generated by both diurnal heating, and from the horizontal and vertical air motions associated with a mid- or upper-level, short-wave trough. The combined processes allow for drier air aloft to mix to the surface replacing the moist boundary layer air. Under these conditions the dryline can mix east for large distances after formation (e.g., McCarthy and Koch 1982; Hane et al. 1993). In contrast, for the quiescent dryline environment, dryline motion is governed largely by turbulent vertical mixing processes as a result of diurnal heating. Under the quiescent regime the dryline typically propagates eastward during the afternoon and retreats back westward at night (e.g., Schaefer 1974a,b; Peterson 1983).

Corresponding author address: Albert Pietrycha, 333 W. University Dr., Romeoville, IL 60446.
E-mail: albert.pietrycha@noaa.gov

Through the use of in situ observations obtained from research aircraft and mobile atmospheric soundings along a north–south-oriented dryline, Ziegler and Hane (1993, hereafter referred to as ZH) produced a conceptual model of the afternoon dryline (see their Fig. 14). In the paper, the authors demonstrated that two parent air masses bound the dryline: a relatively hot, dry quasi-homogenous air mass west of the dryline and a cooler, moist air mass to the east. The interface between the two air masses is termed the mixing zone. Mixing occurs over a horizontal finite width on the order of 10 km. The airmass thermal properties within the mixing zone are composed of thermal variables characterized by mixtures of the two parent air masses.

The 1999 field investigation, a follow-on to the Verifications of the Origin of Rotation in Tornadoes Experiment (VORTEX; Rasmussen et al. 1994) and another in 2000, the Mesoscale Observations of Convective Initiation and Supercell Experiment (MOCISE), addressed, in part, questions pertaining to the thermodynamic variability across the dryline. A total of nine drylines were intercepted using mobile mesonet vehicles (MMVs; Straka et al. 1996). Three meridional drylines that occurred in west Texas on 10 June 1999 and 5 May 2000 are presented herein; two occurred on 5 May 2000. As will be shown, the 5 May 2000 drylines developed in a quiescent environment. The purpose of this paper is to present observations of the horizontal scales of surface features across the dryline that have not been formally documented to date.

The mobile mesonet data obtained on the boundaries revealed some common characteristics. The mixing zone across the dryline was highly variable in width, comprising a series of large horizontal moisture differentials having horizontal scales ranging from 5 km down to several hundred meters. The largest moisture differentials developed when the dryline was nearly stationary: up to 10°C dewpoint differential over 185 m. Concurrent with a deceleration of the dryline to nearly stationary, and while moisture differentials strengthened, surface mesoscale cyclonic circulations with horizontal diameters of 2 km down to less than 300 m were resolved in the data, and visual observations were made of numerous, strongly cyclonically rotating dust devils. All vortices were found to move along or adjacent to the moisture differential zones. Furthermore, at the times the circulations were observed, spatially isolated cumulus clouds located along the dryline exhibited rapid vertical development. Variations in temperature and buoyancy were found to exist. The largest potential temperature (θ), and virtual potential temperature (θ_v) differentials were observed to be 0.9°C over 300 m, collocated with a vortex, and 1.1 K over 1 km, respectively. Following this introduction, section 2 presents data sources and methods. In section 3, data and results are presented with a summary and discussion in section 4.

FIG. 1. Locations of key places mentioned in the text and surface stations utilized for analysis.

2. Data sources and methods

a. Surface analysis

For the regions of interest, hourly surface data from all reporting stations were employed in a subjective surface analysis. Temperature, dewpoint, sea level pressure, and wind fields were included in the analyses. Automated Surface Observing System (ASOS) and Automated Weather Observing System (AWOS) observations generated during the intervening minutes between hourly observations were included in the original analysis. Mobile mesonet data were utilized to augment the analysis. Additionally, a portable weather station located in Spur, Texas (KSPR), the nearest reporting surface station located on the Caprock Escarpment, was included when observations were available (Fig. 1).

Due to the narrow width of a dryline, the ASOS–AWOS data were unable to resolve its location. To minimize location error, the temporal and spatial placements of the boundaries were further determined by tracking narrow bands of cumulus and towering cumulus clouds (if present) at 15–20-min intervals using *Geostationary Operational Environmental Satellite-8* (*GOES-8*) data. Weather Surveillance Radar-1988 Doppler (WSR-88D; Crum and Alberty 1993) data were utilized to track radar ''finelines'' associated with the boundaries, and aided in deriving time-to-space conversion vector orientation. The animation of the *GOES-8* and WSR-88D data aided in determining boundary motion.

An MMV consists of a suite of sensors fastened to the roof of a standard automobile, and a data collection, storage, and display system. The sensor suite records air pressure, temperature, relative humidity, and 3-m wind velocity at 6-s intervals. The reader is referred to Straka et al. (1996) and Markowski et al. (2002) for a complete, detailed description of response time and errors of the mobile mesonet instrumentation specifications. Mobile mesonet transects are executed by separating the vehicles by 0.5–1 km while traveling back

and forth across the dryline. With four MMVs, for example, two traveled east while the other two traveled west, terminating each transect ''leg'' 1–3 km on either side of the moisture differential. Transects were performed almost continuously at speeds between ~2 and ~18 m s^{-1}.

The mobile mesonet data are rigorously quality controlled before any analysis is performed. Quality control procedures are implemented using a series of computer correction algorithms. For data comparison, a 30–60-min time period is selected when the mobile mesonets traveled together in close proximity, <1 km apart, and when meteorological conditions were relatively homogeneous. Data are compared such that any gross reporting errors existing in the mobile mesonet data, whether systematic or periodic, can be analyzed to detect the source of the error. Once the source of the error has been identified, the erroneous data are either corrected or discarded. If the data are in close agreement after comparison with the other MMVs, they are deemed acceptable for analysis.

On 10 June 1999 four MMVs and a mobile Cross-chain Loran Atmospheric Sounding System (M-CLASS; Rust et al. 1990) vehicle (National Severe Storms Laboratory-4; NSSL-4) equipped with similar instrumentation sampled the dryline. Only two MMVs collected data on 5 May 2000. The two MMVs' data quality performance was compared with two other mobile mesonets, as well as NSSL-4, 5 days prior to the 5 May 2000 event during MOCISE when all the vehicles traveled together. Biases were within instrumentation error and the data quality presented herein was deemed acceptable.

The mobile mesonet data can be analyzed, either on a surface map as the data are collected, or a time to space (TS) conversion calculation can be applied (e.g., Fujita 1955; Fujita and Brown 1958; Fujita and Byers 1977). To determine the correct translation vector for the conversion, the most-steady reference frame was computed using a least squares minimization approach [analogous to that used for Doppler radar analysis (Matejka 2002)]. In this study, a large number of potential reference frame motions were systematically examined. The motion resulting in the minimum difference between vector wind observations gathered during a several-minute time window was chosen as the most-steady reference frame motion. In a complex phenomenon such as the boundary layer near a dryline, it should be anticipated that there is a considerable degree of unsteadiness, even during the short time windows used in this study and in the ''most steady'' reference frame. This unsteadiness is partly the result of various flow features propagating differently than other features. A good example might be the dryline moving eastward while vortices along it propagate northward. Hence, some uncertainty is inherent in the details of the analyses presented here, but the two-dimensional maps produced through TS are still vastly more informative than the one-dimensional data obtained by sampling along a highway.

For the MMV observations presented within, the vehicles operated on east–west roads. Due to the use of TS converted space, the MMV observations presented within converge in a V-shape pattern. Because the vehicles performed transects in an east–west direction, the figures depict the oldest (newest) observations at the top (bottom) of the domain (e.g., displacement of the observations is the negative translation velocity). All observations were utilized for the analysis. However, some observations have been omitted from the figures to improve image clarity. Note, a V was used to denote the location of the resolved vortices.

b. Upper-air analysis

Rawinsonde and profiler data were analyzed for both dates. The Midland (KMAF) and Amarillo, Texas (KAMA), soundings, launched at 1200 and 0000 UTC, were closest in proximity to the drylines for the events presented within. The 0000 UTC 11 June 1999 KAMA sounding was not available for inclusion.

c. Remote sensing

The WSR-88D data from KAMA, and Lubbock, Texas (KLBB), were closest in proximity to the drylines. No missing data were encountered for the time periods analyzed. WSR-88D 3-h national mosaic reflectivity imagery, obtained from the National Climate Data Center, were utilized to determine antecedent rainfall prior to both dryline events. *GOES-8* visible satellite imagery, at 15–20-min intervals, was included for analysis when the data were available. Due to parallax errors from *GOES-8*, caution was exercised when depicting cloud features contained within.

3. Data and results

a. 10 June 1999

The large-scale conditions favored a synoptically active dryline on 10 June 1999. A broad mid- and upper-level long-wave trough was located over the western United States with west Texas under a region of increasing westerly mid- and upper-level flow with the approach of a short-wave trough (Fig. 2). Convection from the previous night produced numerous outflow boundaries over the Texas Panhandle and northern New Mexico. The dryline extended south from the point at which it intersected an outflow boundary north of Friona, Texas, to northwest of Hobbs, New Mexico (Fig. 3). The dryline mixed slowly eastward as the afternoon progressed.

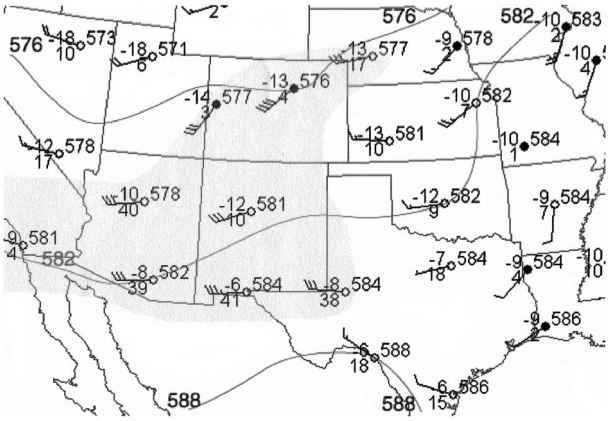

FIG. 2. The 500-mb chart at 0000 UTC 11 Jun 1999 with heights contoured every 6 dam. Standard station model in abbreviated format used: temperature and dewpoint (°C), heights (m), and winds (half barb, 2.5 m s^{-1}; full barb, 5 m s^{-1}; pennant, 25 m s^{-1}). Wind speeds >15 m s^{-1} are shaded.

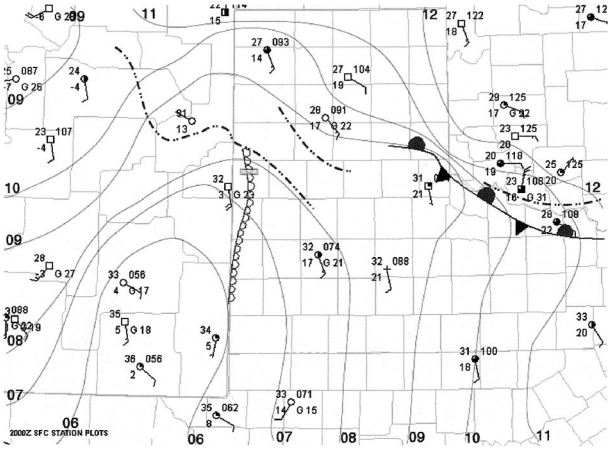

FIG. 3. The 2000 UTC 10 Jun 1999 surface map with subjectively analyzed mean sea level pressure (solid) every 1 mb. Standard station model used: temperature and dewpoint (°C), mean sea level pressure (tens of mb), with the leading 10 omitted; and sky conditions. Winds as in Fig. 2. Dryline, stationary front, and outflow boundaries depicted with conventional symbols. Gray-filled rectangle depicts the location of the mobile mesonet east–west transects as discussed in the text.

MOBILE MESONET OBSERVATIONS

Three MMVs and NSSL-4 intercepted the developing dryline at 1830 UTC, ~10 km west of Friona, (Fig. 1). The road used for transects intersected the boundary at an ~45° angle. The orientation and lack of adequate secondary roads around Friona prevented the MMVs from performing transects normal to the dryline. Land use bordering the road varied between nonirrigated agriculture and commercial development. Elevation varied by less than 5 m at the transect locations on the geological feature known as the Caprock.

Observations commenced at 1830 UTC. During the first hour, moisture differentials along the dryline were initially small; 5°C over 4 km. The dryline moved slowly east at ~3 m s^{-1}. By 1940 UTC (Fig. 4), the observed moisture gradients began to collapse in scale, simultaneous with the development of 1–3-km east-west oscillations in the location of maximum moisture gradients. There was a veering (backing) tendency to the wind in the dry (moist) air, consistent with previous dryline studies. These oscillations persisted for several hours and moisture gradients continued to increase throughout the afternoon at the location where the dryline intersected the highway. Concurrent with the collapse in the scale of the mixing zone, the dryline was observed to become stationary in its forward motion.

WSR-88D data for KAMA at 1957 UTC depicted the location of several outflow boundaries (Fig. 5). No radar fineline was present associated with the dryline. However, a line of small, spatially isolated cumulus clouds visually estimated to be ~2.5 km above ground level (AGL) were observed by the vehicle operators. These clouds were directly above the surface location of the dry-moist axis of the dryline (Fig. 6a).

At 2008 UTC, a cyclonic mesovortex was resolved in the data with a horizontal scale of about 2000 m (Fig. 7). Based on the data in the interval 2004–2020 UTC, the circulation appeared to have been in the process of occluding with respect to the advection of air from the moist side of the dryline to the dry side and vice versa. The vortex was the only one inferred in the 10 June case. Dewpoint gradients in front of the vortex began to strengthen sharply (~9°C km^{-1}). Immediately ahead

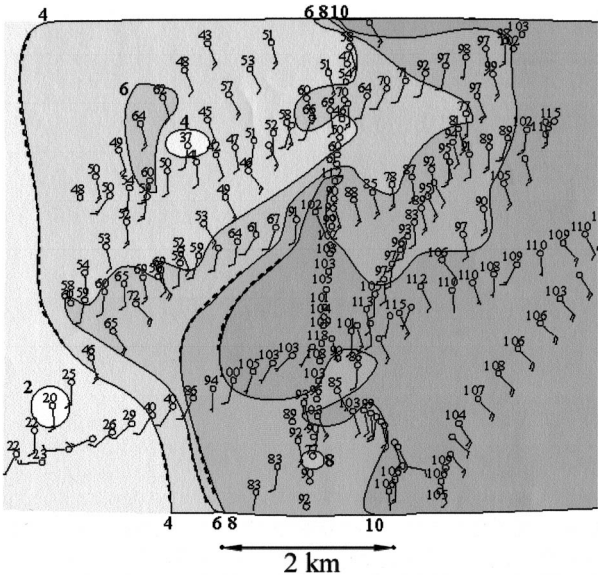

FIG. 4. Subjective analysis of mobile mesonet dewpoint temperature (tenths °C) observations across the dryline at 1938–1956 UTC on 10 Jun 1999. Observations are 18-s averages (three observations) plotted every 18 s using time-to-space conversion with a motion vector from 185° at 6.0 m s^{-1}. Isodrosotherms shaded every 2°C. Winds as in Fig. 2. Dashed contours are used in regions where the analysis is less certain owing to low observation density. The mobile lab is the model with no wind barbs, and the vehicle was stationary during this time interval.

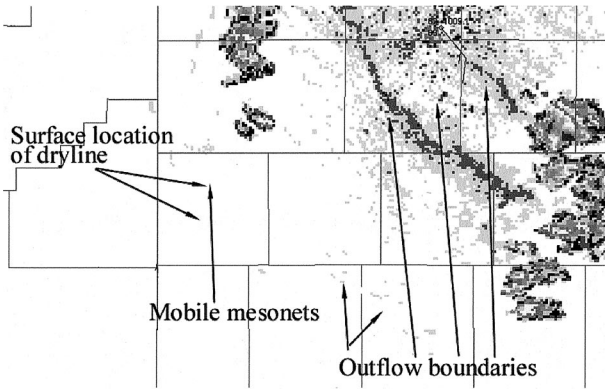

FIG. 5. Base reflectivity from KAMA for 1957 UTC 10 Jun 1999. Pertinent features and locations of the mobile mesonets are depicted.

of the vortex 12°C dewpoints (the largest recorded mobile mesonet values of the day along the dryline) were sampled. Behind the asymmetric vortex, moisture differentials remained large. Of interest, the circulation appeared at the time of strengthening moisture gradients and at the approximate time when the dryline had slowed to nearly stationary.

Concurrently with the increasing moisture differentials and the cyclonic mesovortex between 2004 and 2020 UTC, large dust devils were observed by the mobile mesonet crew. The dust devils moved northward along the axis of maximum moisture gradient at ~6 m s^{-1}. The speed of the dust devils was determined by measuring the time it took for a dust devil to travel between a pair of known points. Some of these dust devils persisted for tens of minutes. The estimated diameters of the largest dust devils were ~80–100 m with heights of >1 + km. In general, no connection could be reasonably inferred between the 12 observed dust devils and individual cumulus clouds.

Fairly persistent moisture gradients on the order of ~6°C km^{-1} continued for the remainder of the transects. Pockets of drier air were sampled at times with no appreciable change in wind velocity or direction juxtaposed with the drier air (Fig. 8). By 2030 UTC the line of cumulus directly over the zone containing the moisture differential and dust devils began to slowly deepen vertically into narrow, towering cumulus clouds, yet these remained spatially isolated (Fig. 6b).

At 2045 UTC, the dryline resumed eastward movement at ~2.0 m s^{-1}. The largest sampled moisture gradient was encountered at ~2100 UTC. Over a 185-m distance, a 10°C dewpoint change was sampled as a mobile mesonet traveled at ~2 m s^{-1} across the dryline (Fig. 9). The associated equivalent potential temperature differential was ~15 K. No vortex was resolved in the data at that time. The towering cumulus clouds still persisted along and now within a 2-km region east of the dryline (Fig. 10a).

The lowest sampled mobile mesonet dewpoint temperature occurred at 2100 UTC (0.6°C). In addition, at

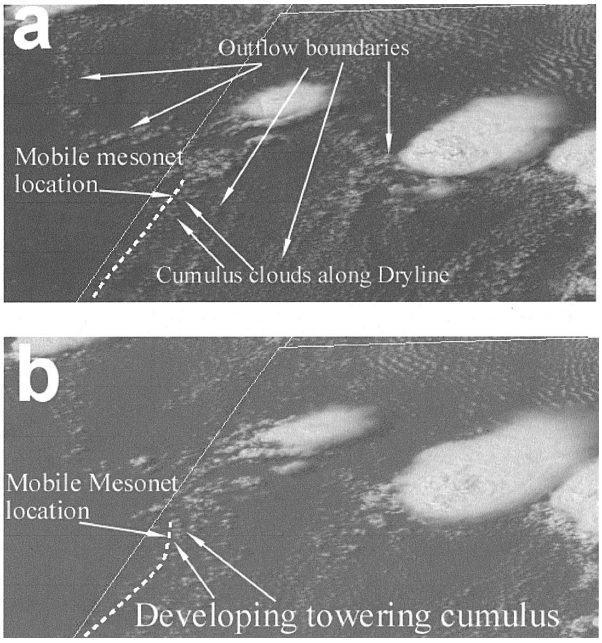

FIG. 6. (a) The 2025 UTC 10 Jun 1999 *GOES-8* visible imagery with approximate locations of the dryline (dash), relevant boundaries, cumulus clouds, and the mobile mesonets depicted. (b) As in (a) except for 2045 UTC.

2100 UTC the Cannon Air Force Base (KCVN) AWOS (a distance of ~58 km west of the leading edge of the dryline) recorded the dewpoint as 1.0°C. The KCVN dewpoint readings oscillated between −1.0° and 2.0°C for the remainder of the afternoon with a sustained

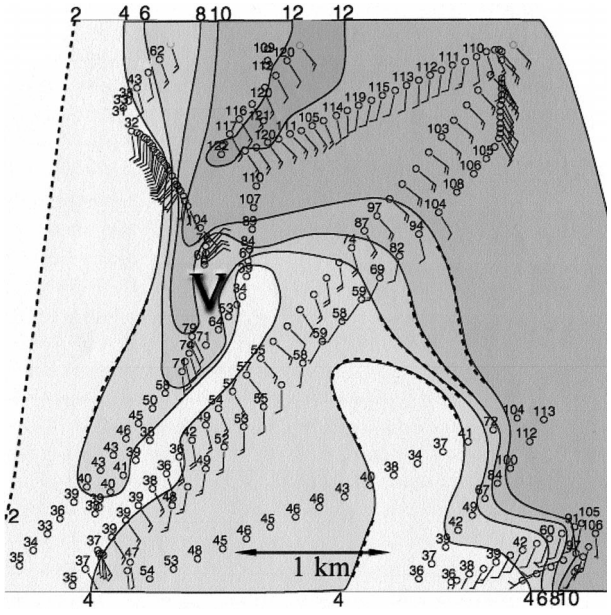

FIG. 7. As in Fig. 4 except for 2004–2020 UTC. Observations plotted every 6 s. The letter V denotes the center of the asymmetric vortex.

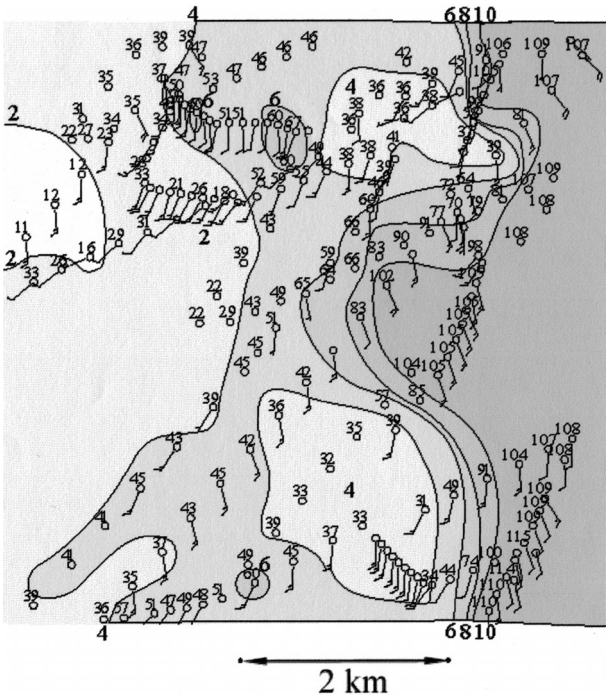

FIG. 8. As in Fig. 4 except for 2020–2033 UTC 10 Jun 1999.

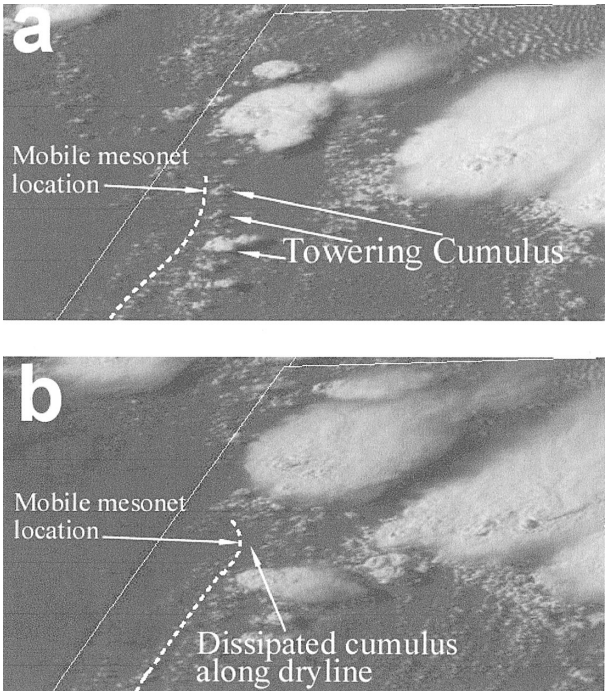

FIG. 10. (a) As in Fig. 6 except for 2132 UTC 10 June 1999. (b) As in (a) except for 2232 UTC.

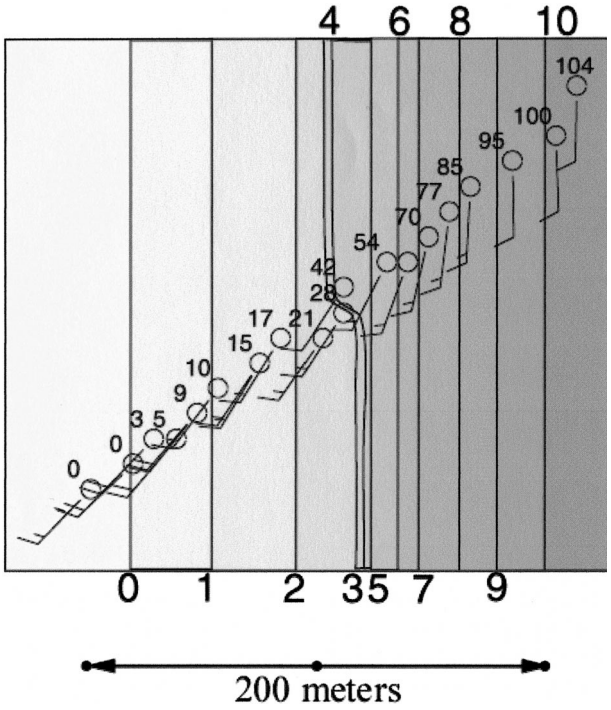

FIG. 9. As in Fig. 7 except for 2100 UTC 10 Jun 1999. No time-to-space conversion was used. The mobile mesonet was traveling northeast at ~2.6 m s^{-1}. Isodrosotherms shaded every 1°C.

southwest wind (Fig. 11). The fact that these well-separated observations behind the dryline contained similar dewpoints suggests that the mobile mesonets were sampling the air mass west of the dryline, and that at the location of the mobile mesonets along the dryline, the mixing zone had collapsed to tens of meters.

Other large thermodynamic differentials sampled along the dryline on 10 June 1999 included the largest θ differential of 1.1°C over 500 m. The largest θ_v differential (1.1 K over 1 km) was collocated with the θ gradient. It cannot be refuted that yet larger thermodynamic differentials might have been sampled had the mobile mesonets performed longer transects east of the dryline.

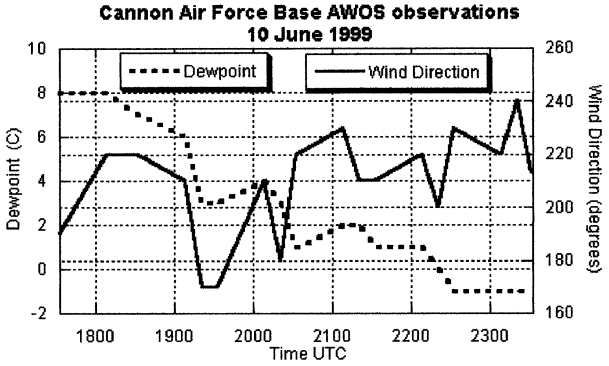

FIG. 11. Time series of Cannon Air Force Base (KCVN) dewpoint (dash; °C) and wind direction (solid) for 1755–2355 UTC 10 Jun 1999.

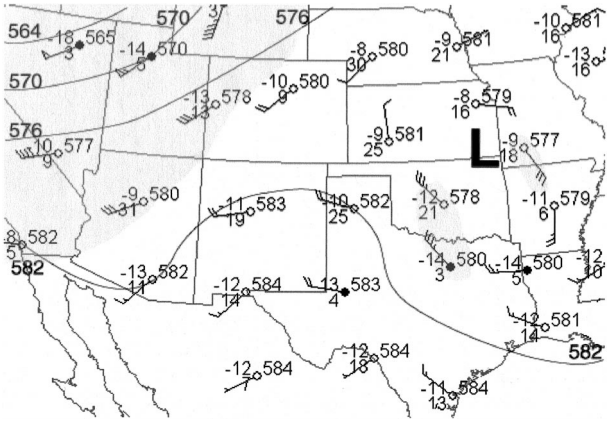

FIG. 12. As in Fig. 2 except for 0000 UTC 6 May 2000.

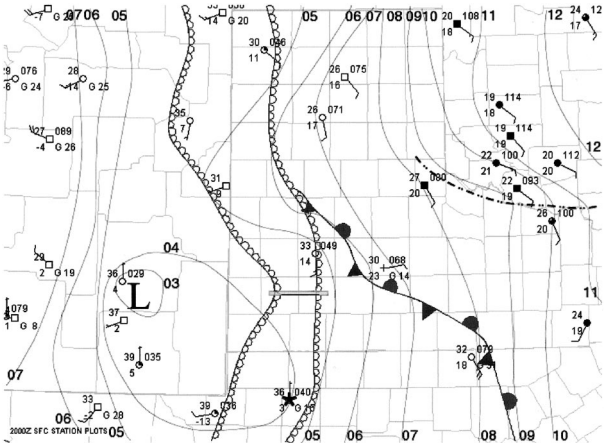

FIG. 13. As in Fig. 3 except for 2000 UTC 5 May 2000. The asterisk denotes the location of the Midland, TX, soundings.

Shortly after 2200 UTC at the location of the mobile mesonets, the dryline began to surge eastward at ~8 m s^{-1}. As the dryline propagated east, the moisture gradient weakened to 4°C km^{-1} (not shown). The towering cumulus dissipated with few cumulus remaining along the leading edge of the dryline. Thunderstorms had, however, developed along and east of the dryline, 35 km south of the mobile mesonets (Fig. 10b). Transects were terminated at 2240 UTC.

b. 5 May 2000

On 5 May 2000, weak tropospheric flow existed over west Texas on the backside of the departing upper-level low (Fig. 12). By early afternoon, drier air hard mixed to the surface in eastern New Mexico with a broad moisture transition present across west Texas (Fig. 13). As will be shown, two distinct drylines developed over west Texas that afternoon.

In contrast to the 10 June 1999 dryline, the 5 May 2000 drylines developed within a quiescent environment. It appears the motions of the drylines were dominated by vertical mixing processes related to the diurnal cycle. Strong afternoon heating allowed mixing to transport dry air to the surface replacing the moist boundary layer air with drier air, which led to the development and eastward propagation of the drylines during the day with rapid westward retreat during the evening. The 0000 UTC 6 May KMAF sounding (Fig. 14), released between the two drylines, indicated deep vertical mixing. Nearly dry-adiabatic conditions existed from the surface up to 458 mb.

MOBILE MESONET OBSERVATIONS

Data collection was limited owing to the availability of only two MMVs for the event. As a result, many of the features presented herein were undersampled. The mobile mesonets operated for more than 5 h between 1900 and 0000 UTC. Land use at the mobile mesonet transect locations across the western dryline was nonirrigated grass/rangeland containing mesquite and low-growing cactus. Irrigated and nonirrigated agricultural land use existed at the eastern dryline mobile mesonet transect locations. The elevation at both drylines varied by less than 25 m atop the Caprock. Mobile mesonet east–west transects were nearly normal to both drylines, at nearly the same latitude, continuous, and obtained at speeds that ranged between ~2 and ~18 m s^{-1}.

The MMVs approached the western dryline from the moist side, around 2030 UTC, 13 km east of Tokio, Texas (Fig. 1). As the vehicles intercepted the dryline, several dust devils less than 20 m in horizontal diameter were visually observed. The dust devils traveled north at 5–6 m s^{-1}. No dust devils were observed away from the dryline. A dewpoint differential of 6.8°C over 3 km was sampled across the dryline (Fig. 15). The lowest sampled dewpoint temperature west of the dryline measured −7.1°C.

The data resolved a northward-moving vortex with

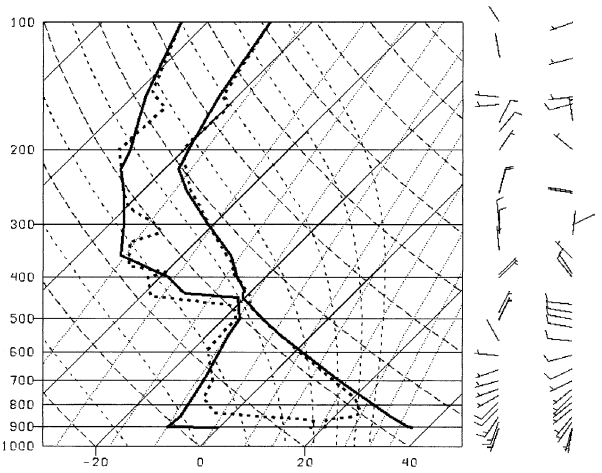

FIG. 14. Skew *T*–log*p* diagram depicting the 1200 UTC (dot) 5 May and 0000 UTC (solid) 6 May 2000 Midland soundings. Pressure in mb, temperatures in ° Celsius, and winds as in Fig. 2.

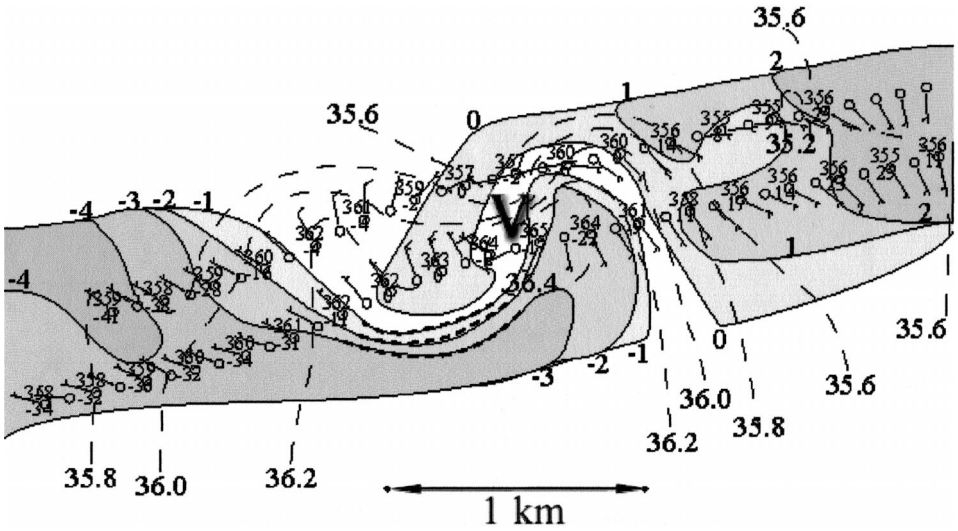

FIG. 15. Subjective analysis of mobile mesonet dewpoint temperature and air temperature (tenths °C) observations across the western dryline at 2032–2035 UTC 5 May 2000. Observations plotted every 6 s using time-to-space conversion with a motion vector from 115° at 4.0 m s^{-1}. Isodrosotherms (shaded) every 1°C and isotherms (dash) every 0.2°C. The vortex had a horizontal scale of approximately 300 m.

an approximate horizontal diameter of 300 m (Fig. 15). The vortex was embedded within the moisture axis. Similar to the 10 June 1999 vortex, the vortex appears to have been in the process of occluding with respect to the advection of air from the moist side of the dryline to the dry side and vice versa. Temperature analysis revealed the vortex was also embedded within a 0.9°C (300 m^{-1}) thermal gradient. This would be the only vortex sampled on 5 May 2000 embedded within a large temperature gradient. Multiple transects of the vortex were not performed.

Transects continued across the western dryline through 2100 UTC. During the 30-min time period the dryline moved east at less than 3 m s^{-1} while the dewpoint gradient remained nearly constant at ~2.3°C km^{-1} (Fig. 16). Differentials of θ and θ_v, and mixing ratio (q), across the 4-km-wide boundary were approximately 1.0°C, 0.5 K, and 2.1 g kg^{-1}, respectively. The thermodynamic differentials were in general agreement with those found in some earlier dryline studies: θ_v, 1.5 K (6 km)$^{-1}$; q, 3 g kg^{-1} across 5 km (e.g., NSSP Staff 1963; ZH; Crawford and Bluestein 1997; Atkins et al. 1998; Ziegler and Rasmussen 1998).

Cumulus fields west of a dryline have been observed in previous dryline studies (Ziegler and Rasmussen 1998). Similarly in this case, a cumulus field was observed to develop in the low relative humidity air along and west of the western dryline. Cloud bases were visually estimated to be ~4.5–5 km (AGL). The estimation was consistent with KMAF's 0000 UTC sounding (Fig. 14), where the lifting condensation level (LCL) and level of free convection (LFC) values for a surface-based parcel were both at 458 mb (~5 km AGL at the locations of the MMVs). The cumulus field would persist and slowly propagate east behind the western dryline for the remainder of the day (Fig. 17a).

Shortly after 2100 UTC the MMVs traveled east to intercept the eastern dryline. Observed dewpoint temperatures between the two drylines, a 70-km distance, varied between ~0.4° and 4.1°C (Fig. 18). Winds within

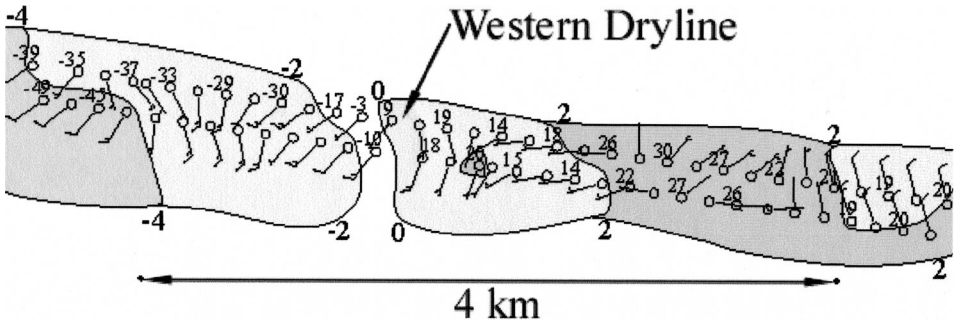

FIG. 16. As in Fig. 15 except for the time 2058–2101 UTC 5 May 2000. Isodrosotherms shaded every 2°C.

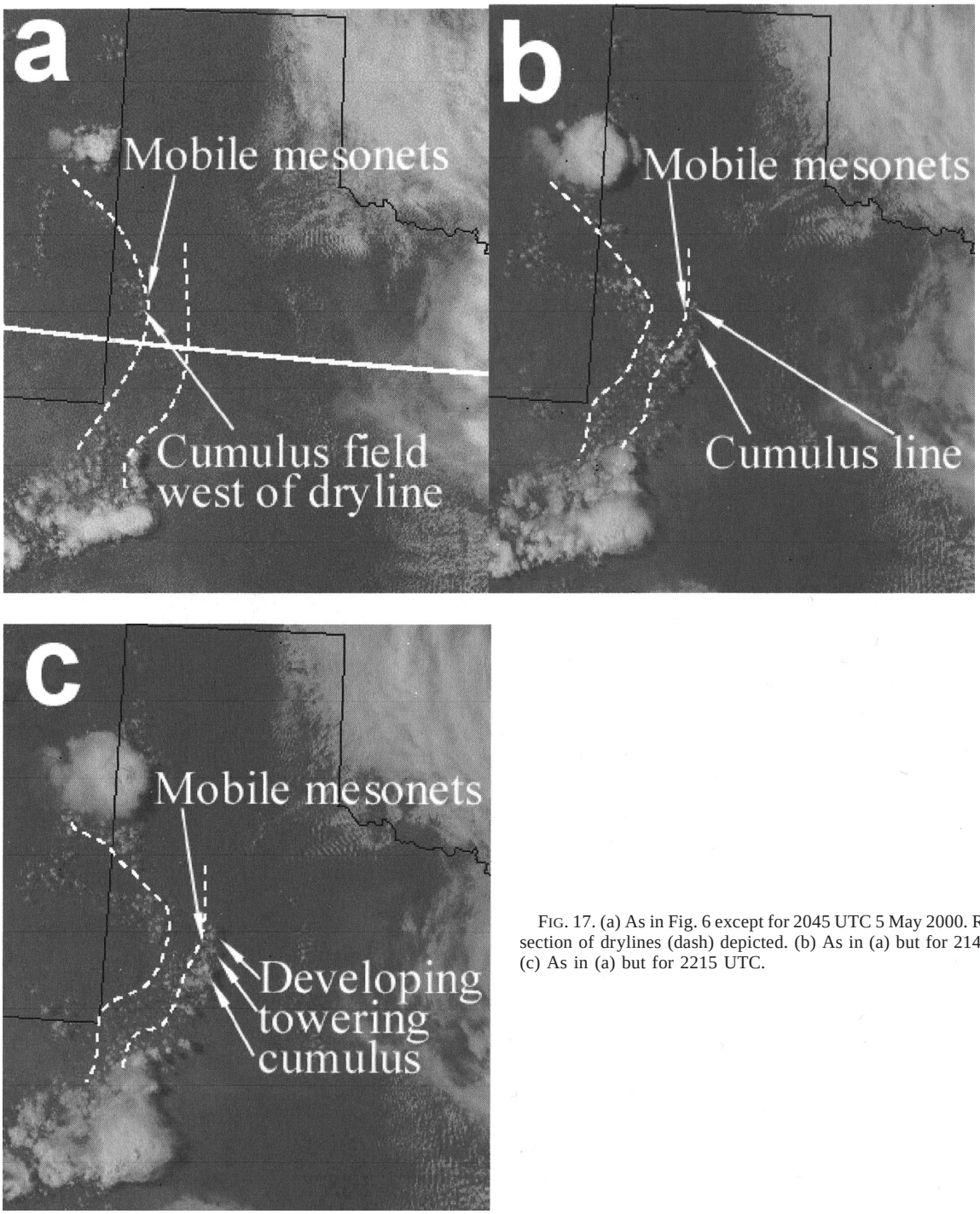

FIG. 17. (a) As in Fig. 6 except for 2045 UTC 5 May 2000. Relevant section of drylines (dash) depicted. (b) As in (a) but for 2145 UTC. (c) As in (a) but for 2215 UTC.

this region were generally light and variable. Mobile mesonet operators observed within the region separating the two boundaries the development of small, flat, infrequent cumulus fractus. Based on MMV operator visual observations, shortly after development the clouds quickly evaporated.

At approximately 2145 UTC, the MMVs intercepted the eastern dryline 10 km east of Tahoka, Texas (Fig. 1). Dewpoints rose 8°C over a 5-km distance across the eastern dryline, and a line of small, spatially isolated cumulus clouds was visually observed above the surface moisture gradient (Fig. 17b). Shortly after transects began, the mixing zone rapidly contracted in horizontal scale (Fig. 19) with increasing dewpoint differentials (>8°C across 2 km). Relatively large dewpoints existed east of the dryline, where small pockets of 10°C were

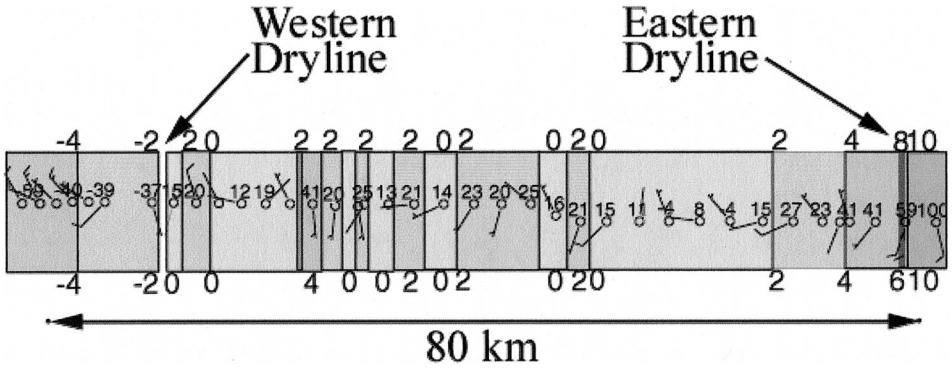

FIG. 18. As in Fig. 16 except for 2040–2154 UTC 5 May 2000 in the region separating the two drylines. Observations plotted every 84 s. No time-to-space conversion was used. The image should not be viewed as if the thermal fields and position of the drylines were steady state.

sampled. The eastern dryline was observed to be nearly stationary at this time after its prior eastward propagation (as detected by visible satellite and WSR-88D imagery) earlier that afternoon.

By 2215 UTC the line of spatially isolated cumulus clouds along the eastern dryline was in a region ~1 km east of the surface boundary and began to develop into towering cumulus with no visible eastward motion (Fig. 17c). The cloud bases were visually estimated to be slightly below 2 km AGL. Given that the moisture gradients were increasing and that the dryline was nearly stationary, it is plausible the cumulus clouds were atop ascending plumes emanating from the surface dryline.

Between 2217 and 2221 UTC, the mobile mesonet data resolved a vortex (Fig. 20). The vortex was located in the relatively drier surface air and along the western edge of the large moisture gradient. It was also during this time frame when numerous ~30–40 m diameter dust devils were observed to develop quickly. The dust devils traveled north along the boundary at ~5 m s^{-1} and persisted for several minutes. Also during this time period, the dryline moved west and moisture differentials continued to contract in scale (dewpoint differential of 8°C in 700 m; not shown).

The mobile mesonet data between 2238 and 2253 UTC indicated moisture differential variations were largest for the event during this time period, with dewpoint differentials reaching ~13.8°C across 400 m (Fig. 21). The dryline continued to remain nearly stationary at the location of the mobile mesonets and no vortices were resolved along the large moisture differential. Dewpoints of −3.9°C were sampled on the west side of the dryline by the mobile mesonets. Based on the observed ~0.1°C to 3.5°C dewpoints across the region separating the two drylines (Fig. 18) and the −3.9°C dewpoints at the eastern dryline, it is believed that the mixing zone had collapsed down to its smallest horizontal scale of less than 400 m. It was also during the same period when small-diameter towering cumulus be-

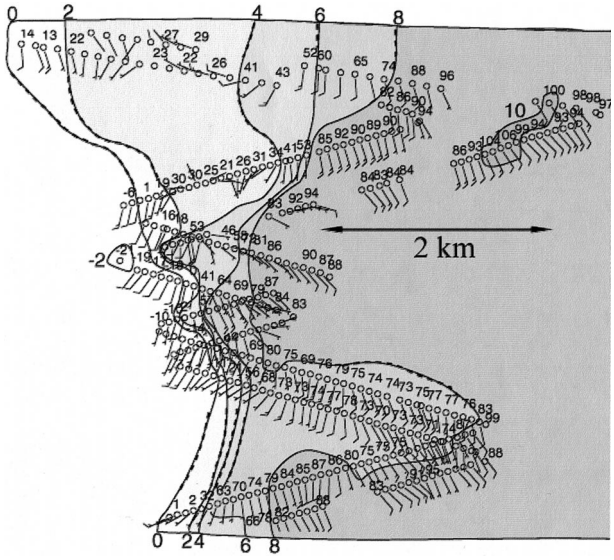

FIG. 19. As in Fig. 16 except for 2144–2203 UTC 5 May 2000 using time-to-space conversion with a motion vector from 175° at 5.0 m s^{-1}.

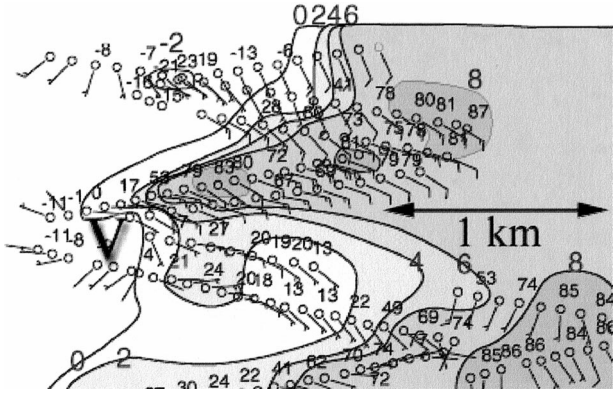

FIG. 20. As in Fig. 16 except for 2217–2221 UTC 5 May 2000 using time-to-space conversion with a motion vector from 175° at 3.0 m s^{-1}.

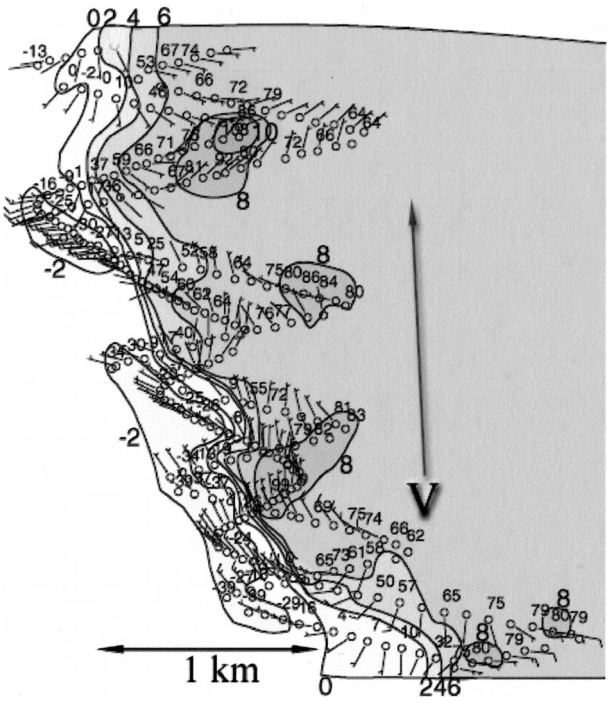

FIG. 21. As in Fig. 20 but for 2238–2253 UTC 5 May 2000. The letter V represents the approximate center of the parent circulation. The arrow denotes the vortex direction of motion.

gan to lose their spatial isolation and consolidate along the dryline.

A large dust devil was observed during the same time period. The dust devil, ~50 m in diameter and ~300 m tall, moved north along the dryline ~1 km inside the deeper moisture, east of the large moisture differential. The dust devil broke down into numerous subvortices, and then, into discrete separate circulations before contracting back into one coherent vortex. Under the assumption that dust devils occur in the central region of a larger vortex (Kanak et al. 2000), and assuming the larger vortex was symmetric, the closest approach by a mobile mesonet to the center of the dust devil was ~600 m within the western periphery of the parent circulation (Fig. 21). It is possible the larger vortex was asymmetric. However, the data are insufficient to determine the degree of symmetry of the parent vortex.

Between 2252 and 2310 UTC, the dryline mixed 3 km east in the 3–4-min period between mobile mesonet transects (Fig. 22). The 3-m mobile mesonet winds exhibited large variability in both speed and direction immediately prior to the eastward dryline motion. Moisture differentials were observed to be smaller during and after the propagation; dewpoint differentials were <8°C across 1 km. As the eastern dryline began to propagate east, a pocket of 1°–6°C dewpoints ~1 km across were bounded east–west by −3° to 0°C dewpoints. It is unlikely the pocket of higher dewpoints was the result of evapotranspirative moisture flux from irrigated land as nonirrigated agricultural land existed at and adjacent to

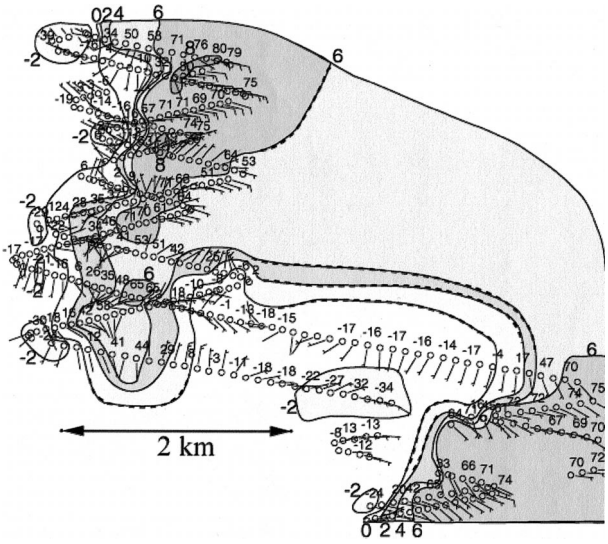

FIG. 22. As in Fig. 20 except for 2252–2310 UTC 5 May 2000.

that location. The observations suggest nonuniform mixing of drier air from aloft to the surface occurred at the locations of the mobile mesonet. No dust devils were visually observed. As the dryline mixed east, the towering cumulus above the boundary rapidly dissipated.

The MMVs continued transects across the eastern dryline. Between 2323 and 2345 UTC the dryline was observed to propagate a second time to the east (Fig. 23). Moisture differentials continued to weaken, now 7°C across 3–4 km. Of interest, the boundary mixed eastward at a time when 2.5–7.7 m s^{-1} southeasterly flow was occurring across and west of the moisture differential. The observations are in contrast to what has been typically observed with dryline studies (e.g., ZH; Crawford and Bluestein 1997; Atkins et al. 1998; Hane et al. 2001): westerly surface winds behind a dryline prior to and/or at the time when forward propagation

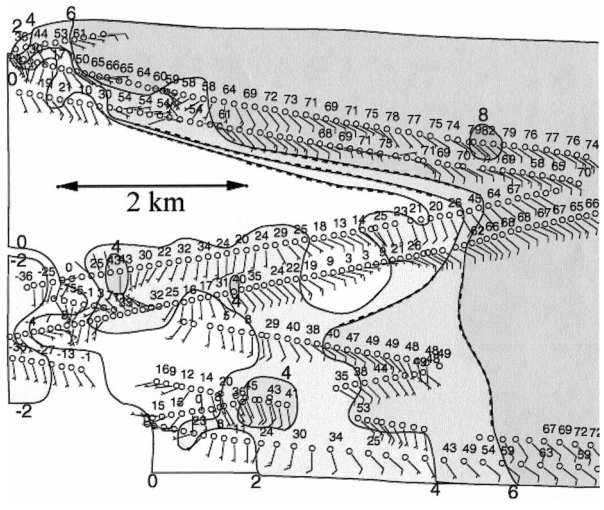

FIG. 23. As in Fig. 19 except for 2323–2345 UTC 5 May 2000.

of a dryline was observed. The limitations of the data in this study preclude any explanations of the southeasterly flow behind the advancing dryline. During this final observation period, no cumulus clouds were observed above or to the east of the boundary. Furthermore, no dust devils or other vortices were observed visually or resolved in the data. Transects were terminated shortly before 0000 UTC.

4. Summary and discussion

The mobile mesonet observations collected from the 10 June 1999 and 5 May 2000 drylines have documented some phenomena that were common to the cases. In this admittedly small sample of drylines, lines of small, spatially isolated, cumulus clouds were observed when large moisture gradients developed across the drylines and when the drylines were nearly stationary. The cumulus eventually grew vertically into towering cumuli at times when mobile mesonet data-resolved vortices and dust devils occurred. Cloud dissipation was observed in tandem with sudden increases in dryline motion and weakening moisture gradients. To our knowledge, these phenomena have not been documented previously. It is hoped that the detailed datasets obtained by the International H_2O Project (IHOP; Weckwerth et al. 2004) may shed more light on how common these phenomena, and the time sequence of evolution, are in a larger sample.

Ziegler and Rasmussen (1998) suggest that, in order to form deep convection, moist boundary layer air parcels must be lifted to the LCL and LFC prior to leaving a mesoscale updraft. Wilson et al. (1992) presented evidence that deep, moist convection may form at the intersection of a convergence zone with horizontal convective rolls; updraft enhancement occurs at these intersections. Atkins et al. (1998) produced evidence that the dryline contains large horizontal variability in the along-line direction. They hypothesized that the variability was due to the interaction of horizontal convective rolls with the dryline. At the point where horizontal convective rolls intersect the dryline, localized updrafts are enhanced and clouds are initiated. Although the data on 10 June 1999, and 5 May 2000 were not collected in the horizontal along-line direction, horizontal convective rolls were not detected in the KAMA or KLBB radar data near the portions of the drylines sampled by the mobile mesonets for either event (Fig. 5).

Several cyclonic vortices were encountered along the drylines. Further questions arise when viewing the varying horizontal scales and temporal evolution of the vortices. What ramifications, if any, they have for convection initiation remains in question. To address these questions, the forcing mechanisms driving the vortices must first be understood. The data are insufficient to determine if a vortex was centered in an updraft or straddling the up–down interface along the dryline. With this dataset, we can only document the existence of the vortices, not their forcing.

What ramifications, if any, the vortices have for convection initiation remains in question. It is possible that vortices along the dryline play a role in the production of localized updraft enhancement. As an air parcel ascends within a vortex, mixing is inhibited, as it is known that helical flows are associated with suppressed turbulence (Andrè and Lesieur 1977; Tsinober and Levich 1983). This in turn could allow the parcel to reach the local LCL and perhaps LFC with greater potential buoyancy, thereby promoting the initiation of deep moist convection that might otherwise not have developed. Whether any evidence can be produced to indicate the vortices enable a more undiluted ascent versus points along the dryline not associated with vortices remains to be investigated.

In addition, in these three cases the mobile mesonet-resolved vortices and visually observed dust devils occurred only at times when the dryline became nearly stationary and while the moisture differentials strengthened. However, moisture differentials also were observed to strengthen independent of the presence of vortices (although it cannot be refuted that vortices were present but not resolved in the data). No vortices were sampled during periods of rapid dryline movement; rapidly moving drylines are difficult to adequately sample with mobile mesonets. Therefore the lack of sampled vortices does not imply their absence.

Many questions remain as to the genesis and toward what effects, if any, the small-scale vortices have on the vertical motion along the dryline. As stated previously, when the drylines were nearly stationary or when large moisture gradients were observed, towering cumuli were also observed. When the dryline was moving or when the moisture gradients were not as strong, cloud dissipation occurred. The observations imply that upward vertical motion was enhanced (diminished) when the drylines were stationary (moving) or when the horizontal moisture gradient was strong (weak). Thus, the following questions are offered for future research considerations. Could locally backed winds north of the vortices act frontogenetically by strengthening the low-level equivalent potential temperature gradient? Could this process explain the increase in upward vertical motion, as evidenced through the towering cumuli, when the gradient was relatively strong? Conversely, could this process explain the diminished upward vertical motion when the gradient was weakening and experiencing frontolysis? Finally, are the vortices the result of developing local convective updrafts forced initially by purely thermodynamic considerations, and enhanced by the resultant tilting and stretching of ambient horizontal local vorticity? Answers to these questions would not only further our understanding of the dryline but also provide operational usefulness toward forecasting convection initiation.

Both ZH and Ziegler and Rasmussen (1998) produced

conceptual models of the dryline during the afternoon and early evening utilizing aircraft data; ZH defined the line-normal horizontal length scale of the dryline above the surface layer to be on the order of 10 km, while Ziegler and Rasmussen documented 1–10 km. On 10 June 1999 and 5 May 2000, at the locations of the mobile mesonets, the dryline horizontal moisture gradient contracted down to several hundred meters. The smaller surface length scale across the dryline compared to previous studies is attributed to the more detailed temporal and spatial sampling by mobile mesonets. Further, it is possible that dryline scale contractions occur more strongly in the surface layer compared to aloft. In the ZH and Ziegler and Rasmussen aircraft studies, the aircraft had an effective sampling interval of ~100 m due to 1-Hz observations at cruise speed. Also, the chilled mirror dewpoint sensor had a slow impulse response and a hysteresis, preventing measurement of large differences over small distances less than ~500 m. Therefore, the actual gradients in those cases could have been larger (C. L. Ziegler 2003, personal communication).

Of interest was the presence of larger low-level moisture content that existed between the western and eastern drylines. Through what processes did the low-level air parcels between the two drylines retain greater humidity compared to the drier surface parcels observed west of the western dryline? Is it possible that the larger low-level moisture levels east of the western dryline were due to the effects of evapotranspiration from local vegetation and soil moisture? Numerical simulation studies have shown that dryline moisture gradients are highly sensitive to horizontal soil moisture and vegetation type (Lanicci et al. 1987; Ziegler et al. 1995; Shaw et al. 1997; Grasso 2000); constant horizontal soil moisture and nonvarying vegetation type lead to small moisture gradients across a dryline. National mosaic radar reflectivity imagery data indicated that, prior to 5 May, it had been more than 72 h since west Texas received precipitation. The higher surface dewpoints, therefore, could be due to the surface flux of water vapor released through vegetative transpiration. However, evaporation from spray-type irrigation superimposed on to the ambient environment cannot be completely ruled out as an additional moisture source. Discussion of the variety and density of vegetation across the region of the western dryline that could have produced the observed surface water vapor flux differential is beyond the scope of this paper.

Several recommendations are offered to aid the operational community in forecasting convection initiation along the dryline. With the increasing availability and number of surface stations reporting in near–real time (i.e., mesonets, school nets, Automatic Position Reporting System Weather Network), forecasters are better equipped to closely monitor the development and progression of the dryline. As shown by McCarthy and Koch (1982), surface instabilities along a dryline can be resolved using high spatial and temporal surface data. With the improving spatial density of observations, forecasters may be able to resolve vortices along the dryline in near–real-time, particularly when the dryline is quasi stationary. Furthermore, the use of 7-min GOES rapid scan operation visible satellite data should aid in the early detection of cumulus development and growth along the dryline. As documented by Pietrycha and Manross (2003), the WSR-88D can resolve vortices along surface boundaries; vortices exhibited 3–6-km horizontal diameters with a wavelength of ~12 km. With the proposed addition of faster volume coverage patterns and tilts of lower elevation angle, the detection of such vortices may further improve (e.g., Brown et al. 2000; Zrnić and Zahrai 2003). Finally, as operational model data assimilation and spatial resolution improve, objectively analyzed fields should prove very useful for alerting the forecaster toward areas to monitor closely along the dryline for convection initiation (i.e., convective inhibition, boundary layer mass convergence and thermal fluxes, etc.). By utilizing these data in concert, it is believed a greater lead time for the detection of convection initiation can be achieved.

Acknowledgments. We are most grateful for the extensive comments by Drs. Paul Markowski, Arthur Doggett, Conrad Ziegler, and three anonymous reviewers. A sincere thank you to Christina Hannon and Elke Edwards for their assistance in preparing this manuscript, Dr. Dave Rust for equipment procurement, the Oklahoma Climate Survey for the radar data, and Marty Mullen, Loren Phillips, Bruce Haynie, and Ed Calianese for the Spur, Texas, observations. We are indebted to the numerous field project volunteers, for without them data collection would not have been possible. Partial support for this research was provided by the National Science Foundation through Grants ATM-9617318, ATM-0003869, and ATM-0340639.

REFERENCES

Andrè, J. C., and M. Lesieur, 1977: Influence of helicity on the evolution of isotropic turbulence at high Reynolds number. *J. Fluid Mech.,* **81,** 187–207.

Atkins, N., R. M. Wakimoto, and C. L. Ziegler, 1998: Observations of the finescale structure of a dryline during VORTEX 95. *Mon. Wea. Rev.,* **126,** 525–550.

Bluestein, H. B., and S. S. Parker, 1993: Modes of isolated, severe convective storm formation along the dryline. *Mon. Wea. Rev.,* **121,** 1354–1372.

Brown, R. A., V. T. Wood, and D. Sirmans, 2000: Improved WSR-88D scanning strategies for convective storms. *Wea. Forecasting,* **15,** 208–220.

Crawford, T. M., and H. B. Bluestein, 1997: Characteristics of dryline passage during COPS-91. *Mon. Wea. Rev.,* **125,** 463–477.

Crum, T. D., and R. L. Alberty, 1993: The WSR-88D and the WSR-88D Operational Support Facility. *Bull. Amer. Meteor. Soc.,* **74,** 1669–1687.

Fujita, T. T., 1955: Results of detailed synoptic studies of squall lines. *Tellus,* **7,** 405–436.

——, and H. A. Brown, 1958: A study of mesosystems and their radar echoes. *Bull. Amer. Meteor. Soc.,* **39,** 538–554.

——, and H. R. Byers, 1977: Spearhead echo and downburst in the crash of an airliner. *Mon. Wea. Rev.*, **105,** 129–146.

Glickman, T. S., 2000: *Glossary of Meteorology.* 2d ed. Amer. Meteor. Soc., 855 pp.

Grasso, L. D., 2000: A numerical simulation of dryline sensitivity to soil moisture. *Mon. Wea. Rev.*, **128,** 2816–2834.

Hane, C. E., C. L. Ziegler, and H. B. Bluestein, 1993: Investigation of the dryline and convective storms initiated along the dryline: Field experiments during COPS-91. *Bull. Amer. Meteor. Soc.*, **74,** 2133–2145.

——, H. B. Bluestein, T. M. Crawford, M. E. Baldwin, and R. M. Rabin, 1997: Severe thunderstorm development in relation to along-dryline variability: A case study. *Mon. Wea. Rev.*, **125,** 231–251.

——, M. E. Baldwin, H. B. Bluestein, T. M. Crawford, and R. M. Rabin, 2001: A case study of severe storm development along a dryline within a synoptically active environment. Part I: Dryline motion and an Eta Model forecast. *Mon. Wea. Rev.*, **129,** 2183–2204.

Kanak, K. M., D. K. Lilly, and J. T. Snow, 2000: The formation of vertical vortices in the convective boundary layer. *Quart. J. Roy. Meteor. Soc.*, **126,** 2789–2810.

Lanicci, J. M., T. N. Carlson, and T. T. Warner, 1987: Sensitivity of the Great Plains severe storm environment to soil moisture distribution. *Mon. Wea. Rev.*, **115,** 2660–2673.

Markowski, P. M., J. M. Straka, and E. N. Rasmussen, 2002: Direct surface thermodynamic observations within the rear-flank downdraft of nontornadic and tornadic supercells. *Mon. Wea. Rev.*, **130,** 1692–1721.

Matejka, T., 2002: Estimating the most steady frame of reference from Doppler radar data. *J. Atmos. Oceanic Technol.*, **19,** 1035–1048.

McCarthy, J., and S. E. Koch, 1982: The evolution of an Oklahoma dryline. Part I: Meso- and subsynoptic-scale analysis. *J. Atmos. Sci.*, **39,** 225–236.

NSSP Staff, 1963: Environmental and thunderstorm structures as shown by National Severe Storms Project observations in spring 1960 and 1961. *Mon. Wea. Rev.*, **91,** 271–292.

Parsons, D. B., M. Hardesty, and R. J. Zamora, 1991: The finescale structure of a West Texas dryline. *Mon. Wea. Rev.*, **119,** 1242–1258.

Peterson, R. E., 1983: The West Texas dryline: Occurrence and behavior. Preprints, *13th Conf. on Severe Local Storms*, Tulsa, OK, Amer. Meteor. Soc., 9–11.

Pietrycha, A. E., and K. L. Manross, 2003: WSR-88D analysis of vortices embedded within a surface low pressure trough and subsequent convection initiation. Preprints, *31st Conf. on Radar Meteorology*, Seattle, WA, Amer. Meteor. Soc., 835–838.

Rasmussen, E. N., J. M. Straka, R. P. Davies-Jones, C. A. Doswell III, F. H. Carr, M. D. Eilts, and D. R. MacGorman, 1994: The Verification of the Origins in Tornadoes Experiment: VORTEX. *Bull. Amer. Meteor. Soc.*, **75,** 997–1006.

Rhea, J. O., 1966: A study of thunderstorm formation along drylines. *J. Appl. Meteor.*, **5,** 58–63.

Rust, W. D., R. P. Davis-Jones, D. W. Burgess, R. A. Maddox, L. C. Showell, T. C. Marshall, and D. K. Lauritsen, 1990: Testing a mobile version of a Cross-chain Loran Atmospheric Sounding System (M-CLASS). *Bull. Amer. Meteor. Soc.*, **71,** 173–180.

Schaefer, J. T., 1974a: A simulated model of dryline motion. *J. Atmos. Sci.*, **31,** 956–964.

——, 1974b: The life cycle of the dryline. *J. Appl. Meteor.*, **13,** 444–449.

Shaw, B. L., R. A. Pielke, and C. L. Ziegler, 1997: The effect of soil moisture heterogeneity on a Great Plains dry line: A numerical study. *Mon. Wea. Rev.*, **125,** 1489–1506.

Straka, J. M., E. N. Rasmussen, and S. E. Frederickson, 1996: A mobile mesonet for finescale meteorological observations. *J. Atmos. Oceanic Technol.*, **13,** 921–936.

Sun, W. Y., and C. C. Wu, 1992: Formation and diurnal variation of the dryline. *J. Atmos. Sci.*, **49,** 1606–1619.

Tsinober, A., and E. Levich, 1983: On the helical nature of three-dimensional coherent structures in turbulent flows. *Phys. Lett.*, **99A,** 321–324.

Weckwerth, T. M., and Coauthors, 2004: An overview of the International H_2O Project (IHOP_2002) and some preliminary highlights. *Bull. Amer. Meteor. Soc.*, **85,** 253–277.

Wilson, J. A., G. B. Foote, N. A. Crook, J. C. Fankhauser, C. G. Wade, J. D. Tuttle, and C. K. Mueller, 1992: The role of boundary layer convergence zones and horizontal rolls in the initiation of thunderstorms: A case study. *Mon. Wea. Rev.*, **120,** 1785–1815.

Ziegler, C. L., and C. E. Hane, 1993: An observational study of the dryline. *Mon. Wea. Rev.*, **121,** 1134–1151.

——, and E. N. Rasmussen, 1998: The initiation of moist convection at the dryline: Forecasting issues from a case study perspective. *Wea. Forecasting*, **13,** 1106–1131.

——, W. J. Martin, R. A. Pielke, and R. L. Walko, 1995: A modeling study of the dryline. *J. Atmos. Sci.*, **52,** 263–285.

——, T. J. Lee, and R. A. Pielke Sr., 1997: Convective initiation at the dryline: A modeling study. *Mon. Wea. Rev.*, **125,** 1001–1026.

Zrnić, D. S., and A. Zahrai, 2003: Evolution of weather surveillance radars: NSSL's perspective. Preprints, *31st Conf. on Radar Meteorology*, Seattle, WA, Amer. Meteor. Soc., 939–941.